ChemComm

COMMUNICATION

View Article Online
View Journal | View Issue

Cite this: *Chem. Commun.*, 2023, 59, 12767

Received 14th August 2023,
Accepted 25th September 2023

DOI: 10.1039/d3cc03930g

rsc.li/chemcomm

In situ real-time neutron imaging of gaseous H_2 adsorption and D_2 exchange on carbon-supported Pd catalysts†

Hamish Cavaye, [a] Christos E. Ballas, [b] Winfried Kockelmann,[a] David Lennon, [b] Paul Collier,[c] Andrew P. E. York,[c] Peter W. Albers[d] and Stewart F. Parker *[ab]

We use *in situ* neutron imaging to observe the adsorption/absorption of hydrogen within a packed catalyst bed of a Pd/C catalyst at a spatial and temporal resolution of ~430 μm and a ~9 s respectively. Additionally, the H_2/D_2 exchange process across the catalyst bed is followed in real time.

Heterogeneous catalysis plays a major role in many industrial processes ranging from commodity chemicals to pharmaceuticals,[1] with hydrogenation reactions having wide application. The particular sensitivity of neutron scattering to hydrogen, has resulted in extensive use of this technique for both *ex* and *in situ* catalyst studies.[2]

Methods to observe in real time what is happening inside a reactor are scarce. X-Ray imaging methods are sensitive to heavy atoms, but insensitive to light atoms such as H, C, N, and O, that are typically the constituents of the reactants and products. Neutron attenuation[3] does not have this limitation as it depends on the total (the sum of the scattering and absorption) neutron cross section. This is both element and isotope dependent[4] and means that light atoms in the presence of heavy atoms are readily detectable. In particular, the large cross section of ^{1}H (82.03 barn, 1 barn = 10^{-28} m^2) means that neutrons are particularly sensitive to hydrogen. For comparison, the total cross sections of ^{2}H, C, N and O are 7.64, 5.55, 11.51, and 4.23 barn respectively.

Neutron imaging methods have long been used to image water flow in fuel cells.[4] More recently, they have been used to study CO_2 methanation, *ortho*-/*para*-hydrogen conversion, methanol synthesis and for combinatorial studies.[5]

Supported palladium catalysts are widely used as hydrogenation catalysts.[6] As a demonstration of the potential of the technique to follow a reaction, here, we use neutron imaging to follow the adsorption/absorption process by successive exposure of a clean Pd/C catalyst to $H_{2(g)}$ and $D_{2(g)}$. Under the conditions of a continuous flow of dihydrogen in the feed stream at 293 K, dihydrogen readily dissociates on the Pd surface and diffuses into the bulk of the Pd crystallite to form β-PdH_x ($x \sim 0.7$).[7] This is the archetypal hydrogen-in-metal system where H/D occupies the octahedral holes in the face centred cubic lattice of Pd metal (the presence of β-PdH_x was confirmed post-reaction using inelastic neutron scattering (INS) spectroscopy (see ESI,† Fig. S1)).

Approximately 8.0 g of Pd (20 wt%) supported on activated carbon (sample 1, present as a fine powder, see ESI† Table S1 and Fig. S2 for the characterisation of the catalysts used) that had been reduced in hydrogen and then the hydrogen desorbed, within a glove box, was placed in an aluminium sample can with a sample thickness of 13 mm. This included connections to allow a flow of gas to enter at the bottom of the sample can, flow through and over the sample, and exit at the top of the can.

Initially, a flow of 100 cm^3 min^{-1} of He at 1.0 barg was allowed to flow over the sample and neutron radiographs were collected. Fig. 1 shows a low noise full-frame neutron radiograph corresponding to approximately 250 s of total exposure time recorded with the IMAT[8] instrument at the ISIS Neutron and Muon Source.

Various parts of the sample can be identified in Fig. 1, including the steel ConFlat® flanges at the top and bottom of the cell together with the steel bolts (the top flange is marked as "a"), that ensure the sample is hermetically sealed by an indium seal and the aluminium cell body ("b"). In the centre of the frame, the catalyst sample can be seen as slightly more

[a] *ISIS Neutron and Muon Source, STFC Rutherford Appleton Laboratory Chilton, OX11 0QX, UK. E-mail: stewart.parker@stfc.ac.uk*
[b] *School of Chemistry, University of Glasgow, Joseph Black Building, Glasgow G12 8QQ, UK*
[c] *Johnson Matthey Technology Centre, Blounts Court, Sonning Common, Reading RG4 9NH, UK*
[d] *Evonik Technology & Infrastructure GmbH, Rodenbacher Chaussee 4, 63457 Hanau-Wolfgang, Germany*

† Electronic supplementary information (ESI) available: Materials and their characterisation; neutron radiography; image processing methods; examples of raw and processed data for samples 1 and 2, neutron image of sample 2 and grey values for selected regions; INS spectra of sample 2 and a reference material. See DOI: https://doi.org/10.1039/d3cc03930g

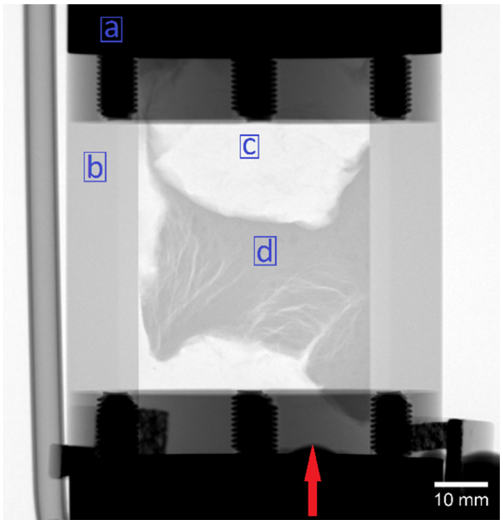

Fig. 1 A low noise full-frame neutron radiograph of sample 1 corresponding to approx. 250 s of total exposure. Various parts of the sample are labelled: (a) steel upper and lower flanges and bolts, (b) aluminium sample cell, (c) silica wool packing, (d) catalyst bed. Red arrow denotes entry point of gas and overall direction of flow.

neutron-attenuating (*i.e.* darker) region ("d"), than the areas around it, which are the silica wool ("c") used to ensure the powdered catalyst does not migrate out of the can during gas flow. It is also possible to see on the left side of the sample there is a small catalyst bed by-pass region, and some parts of the catalyst bed show visible cracks and discontinuities. This inhomogeneity of packing within the bed will affect gas/solid exchange dynamics throughout the region of powered catalyst.

In order to investigate whether the uptake of hydrogen gas could be detected, radiographs were set to be collected repeatedly (approx. 5 s of exposure every 9 s, with a spatial resolution of ~430 μm) and a small percentage of hydrogen gas (5 cm^3 min^{-1}) was entrained into the helium carrier flow (100 cm^3 min^{-1}). Due to the high neutron scattering cross-section of natural abundance hydrogen (referred to as H_2) regions of the sample that adsorb H_2 should increase their neutron attenuation and provide a lower signal, *i.e.*, a lower grey value in the neutron radiographs. In contrast, any exchange of molecular deuterium ($^2H_2$, herein referred to as D_2) for H_2 in the sample should result in an increase in grey value/less neutron attenuation as fewer neutrons are scattered.

The reduced sample 1 was maintained at room temperature with a continuous feed of He at 100 cm^3 min^{-1}; H_2 and/or D_2 were then introduced to the gas feed in the following sequence: (i) H_2, 2 cm^3 min^{-1}, ~9040 s (2.5 h), (ii) H_2, 5 cm^3 min^{-1}; (iii) H_2, 20 cm^3 min^{-1}; (iv) H_2 stopped and catalyst purged with He for ~1200 s (~20 min) to remove gaseous H_2; (v) D_2, 2 cm^3 min^{-1}, ~2760 s (~46 min) (vi) D_2, 20 cm^3 min^{-1}.

The left part of Fig. 2 shows a cropped-frame neutron image of sample 1, with four different regions of interest (ROIs) marked in coloured squares; two covering the silica wool below (black) and above (magenta) the catalyst bed, and two within the catalyst bed itself (blue and green). Of the two ROIs in the catalyst, the blue region is at the bottom of the sample, close to the ingress point of the gas flow, whereas the green region is at the top of the sample and distant from any cracks or bypasses.

The right-hand side of Fig. 2 shows plots corresponding to the average grey values in each ROI for each frame in the collected datasets over time (Savitzky–Golay signal smoothed; representative raw data is available in the ESI,† see Fig. S3 and S4). It is clear to see that the black and magenta ROIs show only a slight variation in grey value over the course of the experiment, remaining within <0.5% of the original value over the course of ~72 000 s (~20 h). This is to be expected, as the silica wool is not thought to interact strongly with the gasses flowing through it. This also shows that the gas phase H_2 is invisible due to its low density.

However, the blue and green ROIs show much more interesting trends. Firstly, for both ROIs, once H_2 begins to enter the system, there is a distinct drop in transmitted neutrons leading to grey values which plateau at around a 2% reduction. This plateau was reached even with just 2 cm^3 min^{-1} flow rate of H_2 and did not reduce further with increased H_2 flow rate (data not shown). For the blue region, close to the bottom of the catalyst bed where the gas enters the system, this drop is very rapid, reaching saturation after ~420 s (~7 min). In fact, the decrease in grey value in this region is essentially instantaneous within the approximately 9 s time resolution of the neutron imaging measurement, with the measured delay up to the sudden decrease likely to reflect the time for the gas switch to be transmitted to the cell from the gas manifold (there are ~10 m of 1/8″ pipe between the manifold and the cell). For the green region, which is at the top of the catalyst bed, this adsorption process takes notably longer, only reaching saturation after ~1800 s (~30 min). This extended delay is thought to indicate resistance to gas flow within the bed and is indicative of catalyst packing density throughout the bed volume. Indeed, the cracks and by-pass regions identified in Fig. 1 facilitate rapid gas exchange in those zones, as indicated by the essentially instantaneous (within the time resolution, ~9 s) gas retention by the solid on contact with H_2.

Eqn (1) seeks to account for these observations:

$$H_{2(g)} \xrightarrow{k_1} H'_2 + 2* \xrightarrow{k_2} 2H_{(ad)} \quad (1)$$

where $H_{2(g)}$ signifies gaseous dihydrogen, H'_2 represents dihydrogen present at a Pd crystallite and k_1 is a rate coefficient that describes the diffusion of dihydrogen gas throughout the catalyst bed. The asterisk is an adsorption site at the surface of the Pd crystallite and k_2 is a rate coefficient that accounts for the dissociative adsorption of dihydrogen. Using half-life as a kinetic indicator, Fig. 2(b) may be interpreted as indicating that under our conditions the adsorption process is universally fast ($t_{1/2} \ll 9$ s) but that the gas percolation throughout the bed can be unimpeded ($t_{1/2} \ll 9$ s) or retarded ($t_{1/2} \sim 15$ min), with the different values illustrating the different bed packing densities within the reactor.

The discontinuous *x*-axis in Fig. 2 denotes time between measurements. After this point, from $t \approx 63\,000$ s ($t \approx 17.5$ h),

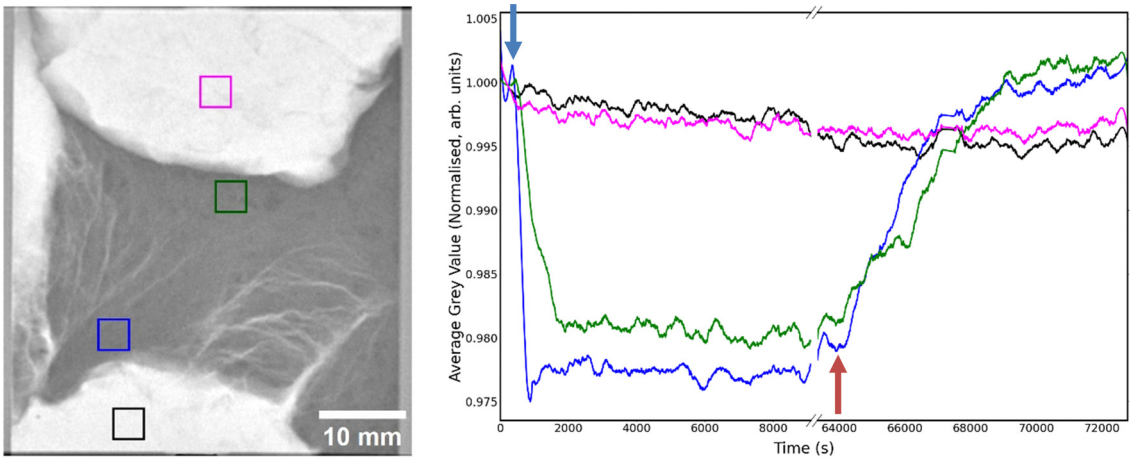

Fig. 2 Left: A cropped-frame neutron radiograph of sample 1 showing just the catalyst area of interest. Each region of interest (ROI) that underwent further analysis is marked in a coloured square. Right: A plot of the average grey value in each corresponding ROI (colours match the ROI from the left figure) *versus* elapsed time. Note the broken *x*-axis showing a gap in data collection time between $H_{2(g)}$ and $D_{2(g)}$ flows. The blue arrow shows approximately when $H_{2(g)}$ flow was initiated. The red arrow shows approximately when $D_{2(g)}$ flow was initiated.

the sample had been saturated with H_2 but was undergoing a purge flow of just He. At approximately t = 64 000 s (17.8 h, as indicated by a red arrow), D_2 is introduced into the carrier gas. For both regions in the catalyst bed (Fig. 2, green and blue boxes), a slow increase in grey value can be seen over the course of approximately 4500–5400 s (75–90 min), which eventually returns to the same level as at the start of the experiment, with both areas exhibiting a $t_{1/2}$ value of ~2475 s (~41 min). Eqn (2) describes the elementary reactions of the spatially resolved H_2/D_2 exchange process visualised in Fig. 2(b):

$$2H_{(ad)} + D_{2(g)} \xrightarrow{k_3} 2D_{(ad)} + H_{2(g)} \quad (2)$$

where k_3 is the rate coefficient for the progressive H/D exchange process at the Pd surface. Thus, we infer that the majority of adsorbed, highly attenuating H_2 is exchanged with the much less attenuating D_2, and that this exchange process is significantly slower than the original adsorption process and the process for the equilibration of H_2 across the whole of the catalyst bed.

To investigate the possibility of a H_2 diffusion/adsorption front, a reference radiograph recorded before H_2 gas dosing was subtracted from each image frame of the H_2 adsorption experiment. This produced a set of "difference" radiographs, highlighting just regions of the data that changed over time.

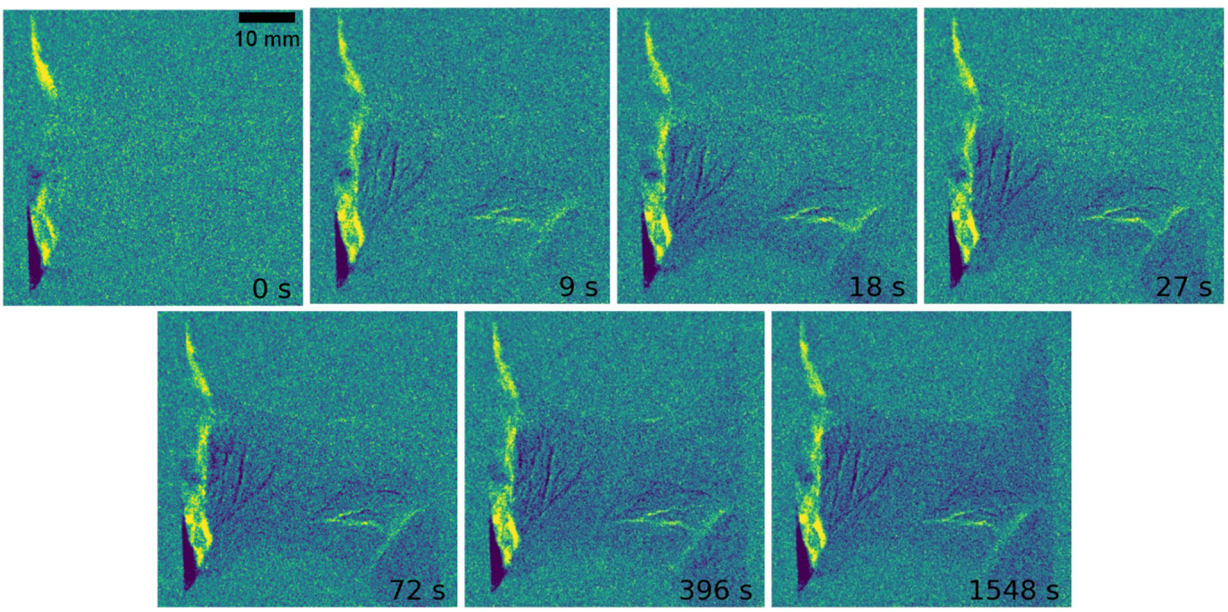

Fig. 3 Selected difference frames of the catalyst bed for sample 1 at various times showing the advancing of a front of H_2 adsorption. Times are approximate and assume 9 s between frames during data acquisition. *NB*: the strong feature on the left-hand side of every frame was caused by an initial shift in the position of some of the catalyst powder upon beginning the gas flow and can be ignored for the purposes of examining H_2 adsorption.

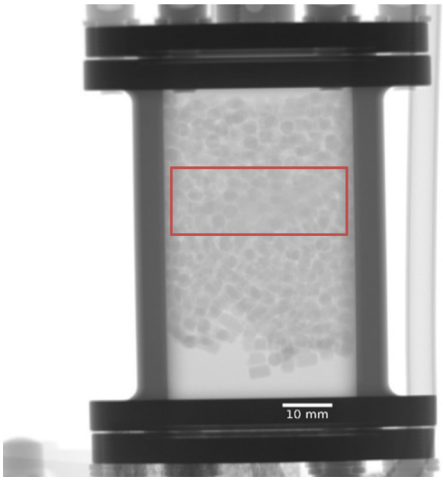

Fig. 4 Full-frame neutron radiograph of sample 3 corresponding to approx. 250 s of total exposure. The red rectangle indicates the region of greatest powdered catalyst concentration.

A video of these data can be seen in the ESI† and Fig. 3 shows selected frames over a period of 1548 s (~26 min). Dark blue regions indicate increased neutron attenuation, caused by adsorption of H_2 gas.

These data demonstrate that H_2 uptake begins in the lower-left corner of the catalyst bed and the gas uptake front advances over time until the entire sample is saturated. Additionally, regions of the catalyst bed that are more accessible due to cracking show faster H_2 uptake, as might be expected.

The measurements for sample 1 were repeated for a second fresh sample of the same 20 wt% Pd/C catalyst (sample 2, mass approximately 7.0 g, see ESI† for additional images and figures, Fig. S5 and S6), and reproduced all of the trends observed for sample 1, confirming the repeatability of the reported outcomes over this representative hydrogenation catalyst.

However, Al has limitations for catalyst studies requiring elevated temperatures and/or pressures. To address this point, preliminary measurements were performed on a different Pd/C catalyst (sample 3, 5 wt% Pd/C, see the ESI†), mass approximately 1–2 g located within a flat stainless steel cell. Here, the Pd/C catalyst powder was located between an upper and lower layer of activated carbon (Norit RX-3 extra) that was present in pelleted form. Fig. 4 shows a low noise full-frame neutron radiograph corresponding to ~250 s of total neutron exposure time and shows the carbon pellets to be readily observable throughout the reactor. The red box in Fig. 4 shows the location of the hydrogen dosed Pd/C powder that is just about discernible as a slightly 'fuzzy' zone in the middle of the reactor. Exchanging D_2 for H_2 in the gas flow led to an increase in grey value (*i.e.*, a decrease in neutron attenuation) within this zone (results not shown). Although the signal was weaker than observed in Fig. 2 (stainless steel being a stronger attenuator of neutrons than Al, plus the lower Pd loading in sample 3), nonetheless this outcome confirms that H_2/D_2 exchange can be directly imaged on a range of catalysts and reactors.

In summary, this work highlights several features of neutron imaging that are valuable for catalyst studies. The progress of a reaction front moving through a catalyst bed is readily observable, which clearly shows the crucial importance of how the catalyst bed is packed. The particular nature of this catalyst means that the ultimate scattering species is identifiable as β-PdH_x, as confirmed by INS. As noted previously,[6] the attenuation of the neutron beam by adsorbed H_2 is readily quantifiable. The difference in kinetics, as indicated by a half-life, between adsorption of H_2 in different regions of an activated catalyst and the exchange of adsorbed H_2 with D_2 are discernible. The first two samples used a relatively high loading catalyst of 20 wt% Pd to maximise the sensitivity, the third was significantly less at 5 wt% but still yielded fair images. Even lower metal loadings may also be accessible. Our first two samples used Al cans because we were concerned about the attenuation by steel. Our third sample shows that this is not overly significant (the transmission is ~70% that of Al) and opens the way for reactions at elevated temperatures and pressures. We also note that the technique lends itself to *operando* measurements.

The STFC ISIS Neutron and Muon Source is thanked for access to neutron beam facilities *via* RB2220700.[9] The assistance of the ISIS Pressure and Furnace section is gratefully acknowledged. The EPSRC are thanked for the provision of a PhD studentship (CB, EP/T517896/1 and EP/W524359/1). Johnson Matthey plc are thanked for project support.

Conflicts of interest

There are no conflicts to declare.

References

1 H.-J. Arpe, *Industrial Organic Chemistry*, Wiley-VCH, Weinheim, 2010.
2 (*a*) A. J. O'Malley, S. F. Parker and C. R. A. Catlow, *Chem. Commun.*, 2017, **53**, 12164–12176; (*b*) X. Yu, Y. Cheng, Y. Li, F. Polo-Garzon, J. Liu, E. Mamontov, M. Li, D. Lennon, S. F. Parker, A. J. Ramirez–Cuesta and Z. Wu, *Chem. Rev.*, 2023, **123**, 8638–8700.
3 N. Kardjilov, I. Manke, R. Woracek, A. Hilger and J. Banhart, *Materials Today*, 2018, **21**, 652–672.
4 P. Boillat, E. H. Lehmann, P. Trtik and M. Cochet, *Curr. Opin. Electrochem.*, 2017, **5**, 3–10.
5 (*a*) A. Borgschulte, R. Delmelle, R. B. Duarte, A. Heel, P. Boillat and E. Lehmann, *Phys. Chem. Chem. Phys.*, 2016, **18**, 17217–17223; (*b*) G. Romanelli, T. Minniti, G. Skoro, M. Krzystyniak, J. Taylor, D. Fornalski and F. Fernandez-Alonso, *J. Phys. Chem. C*, 2019, **123**, 11745–11751; (*c*) J. Terreni, E. Billeter, O. Sambalova, X. Liu, M. Trottmann, A. Sterzi, H. Geerlings, P. Trtik, A. Kaestner and A. Borgschulte, *Phys. Chem. Chem. Phys.*, 2020, **22**, 22979–22988; (*d*) M. Nikolic, F. Longo, E. Billeter, A. Cesarini, P. Trtik and A. Borgschulte, *Phys. Chem. Chem. Phys.*, 2022, **24**, 27394–27405.
6 D. Teschner, Z. Révay, J. Borsodi, M. Hävecker, A. Knop-Gericke, R. Schlögl, D. Milroy, S. D. Jackson, D. Torres and P. Sautet, *Angew. Chem.*, 2008, **120**, 9414–9418.
7 S. F. Parker, H. C. Walker, S. K. Callear, E. Grünewald, T. Petzold, D. Wolf, K. Möbus, J. Adam, S. D. Wieland, M. Jiménez-Ruiz and P. W. Albers, *Chem. Sci.*, 2019, **10**, 480–489.
8 T. Minniti, K. Watanabe, G. Burca, D. E. Pooley and W. Kockelmann, *Nucl. Instrum. Methods Phys. Res.*, 2018, **888**, 184–195.
9 D. Lennon, *et al.*, A neutron imaging study of a working catalyst, STFC ISIS Neutron and Muon Source, 2023, DOI: **10.5286/ISIS.E.RB2220700**.

